Nanoparticles owing to their small size, large surface area and high surface energy, play an important role in electronics, photonics, magnetism, conductor, field effect transistors, semiconductor, medicines, photodetectors, solar cells and in tribology, too [Astruc *et al*.(2010), Weintraub *et al*.(2010), Wu *et al*.(2011), Mirin *et al*.(2010), Huang *et al*.(2013) and Huang *et al*.(2015)]. The nanoparticles such as CuO, ZrO_2, ZnO [Battez *et al*.(2008)], TiO_2 [Zhang *et al*.(2011)], CeO_2 [Bai *et al*.(2014)], $CaCu_{2.9}Zn_{0.1}TiO_{12}$ [Jaiswal *et al*.(2014)], lanthanum borate [Hu *et al*.(2000)] etc. have been investigated as oil lubricant additives. The admixture of these particles with base oil enhances the extreme pressure, antiwear and friction reducing properties of the lubricating base oil.

Being environment friendly, ZnO and MgO nanoparticles [Yang *et al*.(2010)] have been used for the various applications in tribology. Wang *et al*.(2008) have explored the metal-self-repairing behavior of magnesium metal. In addition to this, magnesium palmitate and magnesium stearate based detergents have been used as antioxidant [Mohammed *et al*.(2013)]. The antiwear and antifriction properties of magnesium borate nanoparticles have been reported [Hu *et al*.(2002)]. Since lubricant also acts as a coolant, the thermal conductivity of additive molecules is very important in reducing asperity temperature at the metal-metal interface. The thermal conductivity of MgO NPs is 3.5 folds higher than those of ZnO NPs [Xie *et al*.(2010)]. The potential applications of these ZnO and MgO NPs have prompted us to synthesize the Mg-doped ZnO NPs. The Mg^{2+} ions are readily incorporated into the crystal lattice of ZnO because ionic radius of Zn^{2+} is 0.74 Å which is very close to that of Mg^{2+} ion, 0.72 Å [Yang *et al*.(2010)]. The synthesis protocol for the Mg-doped ZnO nanoparticles as reported by Yang *et al*. (2010) needs specific reaction conditions, however,

the protocol adopted in this investigation is inexpensive and easy to follow under normal conditions.

The present chapter reports the synthesis and characterization of magnesium doped zinc oxide nanoparticles ($Zn_{0.88}Mg_{0.12}O$, ZMO) of different size 27, 39 and 44 nm for ZMO, ZMO-1 and ZMO-2 respectively. The effect of particle size of as prepared ZMOs nanoparticles along with 0.10% SDS in paraffin oil has been evaluated on four ball lubricant tester. It is anticipated that the presence of magnesium as dopant in ZnO NPs may enhance the tribological properties of base lube. In addition to this, it is expected that as the size of these ZMOs NPs decreases their tribological properties increase and thereby the friction and wear properties of paraffin base oil are improved.

7.1. Materials and methods

7.1.1. Chemicals

All materials used in the synthesis were of analytical reagent grade and employed without any further purification. Zinc nitrate hexahydrate (Merck, ≥99.6%), magnesium nitrate hexahydrate (Merck, ≥99%), citric acid anhydrous (Merck, ≥99.5%) and sodium dodecylsulfate (SRL chemicals, ≥99%) were used as precursor.

7.1.2. Synthesis of ZMOs nanoparticles

The synthesis of Mg-doped-zinc oxide ($Zn_{0.88}Mg_{0.12}O$) NPs has been achieved using auto-combustion method [Kalyani *et al*.(2015)]. In this method, zinc nitrate hexahydrate (10.72g) in 20 ml of DD water and Magnesium nitrate hexahydrate (1.22g) in 5 ml of DD water were mixed together. The solution of citric acid (4.69g) in 10 ml DD

water was added to this mixture. The mixed solution was evaporated with continuous stirring at 200±5 °C on a hot plate until it turns into gel and finally burnt. Thereafter, within a few seconds of combustion reaction blackish ash appeared. The obtained ash was calcined at 600 °C in air for 4h. Thus, prepared magnesium doped zinc oxide nanoparticles ($Zn_{0.88}Mg_{0.12}O$) named as ZMO, were further calcined at 800 and 1000 °C for 2h and designated as ZMO-1 and ZMO-2, respectively.

7.1.3. Characterization of ZMOs nanoparticles

The X-Ray diffraction patterns of ZnO and ZMOs NPs synthesized by auto-combustion method are shown in Figure 7.1. Well-defined diffraction peaks for the hexagonal wurtzite phase structure of ZnO are clearly visible in the diffraction pattern of ZnO NPs. Diffraction peaks are located at 31.6°, 34.4°, 36.1°, 47.5°, 56.5°, 62.8°, 66.1°, 67.8°, 68.9°, 72.5° and 76.8° corresponding to the (100), (002), (101), (102), (110), (103), (200), (112), (201), (004) and (202) faces of wurtzite ZnO NPs, respectively (JCPDS No. 36-1451). Absence of any peak due to magnesium oxide in the XRD spectra confirmed the formation of single phase. The average crystallite size of the ZnO, ZMO, ZMO-1 and ZMO-2 NPs was obtained as 30, 27, 39 and 44 nm, respectively using the Debye Scherrer formula:

$$D = k \lambda / \beta \cos\theta$$

Where, λ is the wavelength of the X-ray, k is a constant taken as 0.89, θ is the diffraction angle and β is the full width at half maxima (FWHM). The crystallite size derived from the XRD data revealed that upon doping of magnesium into ZnO, the average

crystallite size of parent ZnO NPs has reduced. Besides this, the average crystallite size of ZMOs NPs increased with increase in temperature.

The TEM micrographs of the synthesized ZMO NPs and the corresponding selected area electron diffraction (SAED) patterns are shown in Figure 7.2. From the TEM images, particle size of ZMO NPs were measured manually using the ImageJ software and the corresponding projected areas of the particles were converted to particle diameters. The average particle size of ZMO NPs is about 25 nm which correlates very well with the size obtained from powder XRD pattern recorded for the same sample. The SAED pattern corresponding to ZMO NPs gives a set of diffraction rings, which can be clearly assigned to the diffractions of the (100), (002), (101), (102), (110), (103) and (200) planes, respectively, of the wurtzite structure of ZnO. These results are consistent with the XRD characterization. The presence of magnesium in the EDX spectra of ZMO NPs also confirms the formation of Mg-doped-ZnO NPs mentioned in Figure 7.3.

7.1.4. Tribological Characterization

7.1.4.1. Sample Preparation

The suspensions of ZMOs NPs having concentration 0.00, 0.25, 0.50 and 1.00 % (w/v) with 0.10% SDS in paraffin oil were made by stirring for half an hour on magnetic stirrer to obtain the uniform mixture. In order to form stable suspension these blends were further sonicated for one hour at room temperature. The entire tests were carried out at an optimized concentration, 0.25% w/v ZMOs + 0.10% SDS.

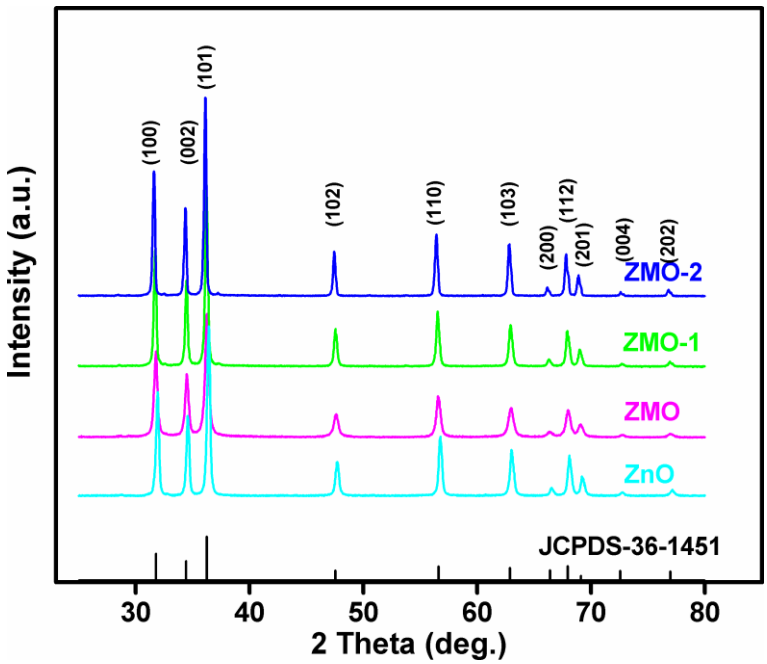

Figure 7.1. Powder X-ray Diffraction pattern of pure ZnO and Mg-doped-ZnO nanoparticles having different particle size

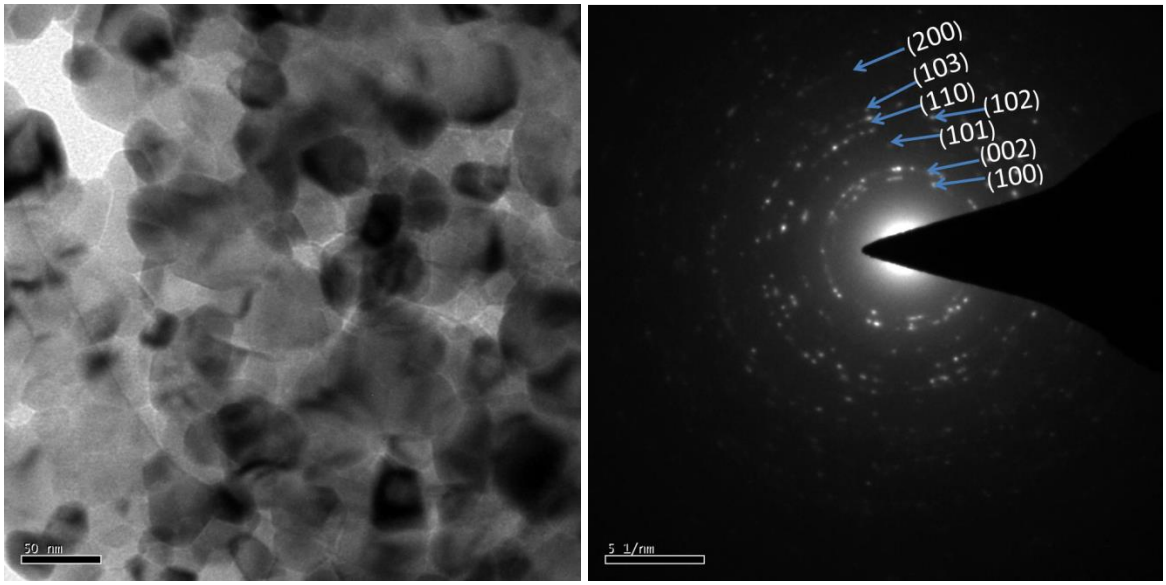

Figure 7.2. TEM-image of ZMO nanoparticles along with selected area electron diffraction (SAED) pattern

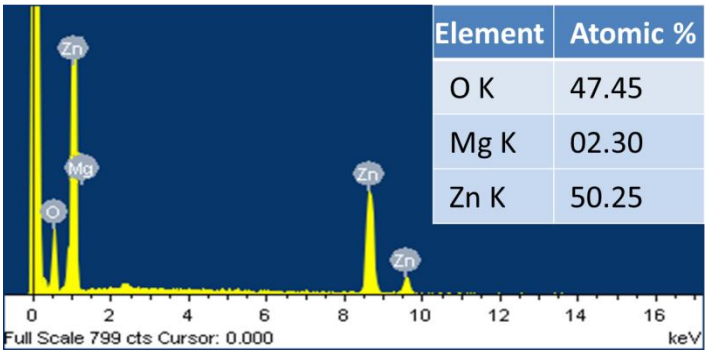

Figure 7.3. Energy dispersive X-ray spectrum showing constituents and chemical composition of ZMO nanoparticles

7.1.4.2. Suspension stability of SZMOs

To investigate the suspension stability of SZMOs NPs in paraffin oil, the optimized concentration of SZMO and SZMO-2 NPs were further diluted 10 times in order to record their UV-spectra. Suspension stability of SZMOs was studied by means of absorbance measurement using UV-Visible spectrophotometer at different time interval.

UV-Visible spectra of SZMOs nanoparticles recorded in the range 300 to 600 nm exhibit a broad band around 360-370 nm confirming the formation of ZMOs NPs [Xiong *et al*.(2009)]. The stability of nanofluids is strongly affected by the characteristics of the suspended particles such as particle morphology and its size in base oil. Besides this, the addition of a surfactant improves the stability of the suspension. The relative stability of SZMOs nanofluids has been investigated with the help of UV-Visible absorption at different time interval. UV-Visible spectrum of SZMOs is shown in Figure 7.4a. With the expense of time, the characteristic absorption of the SZMO NPs displayed hypochromic shift i.e. decrease in absorptivity (in inset). The hypochromicity confirms the initiation of aggregation of SZMOs NPs in suspension. The absorbance of SZMOs NPs in oil

suspensions decreases with increasing sediment time. After 1h, relative concentration of the SZMO NPs remains almost constant till 24h showing the stability of nanofluids, thereafter there is gradual decrease in relative concentration of SZMO nanofluids with time. On the other hand, SZMO-2 NPs are comparatively less stable than those of SZMO. After 48h, relative concentration is maintained over 62% compared to the initial concentration of SZMO NPs. Figure 7.4b exhibits the photographs of SZMOs suspension in paraffin oil at different time duration where it can be clearly seen that after 48h SZMO NPs remain suspended to a greater extent as compared to SZMO-2 NPs.

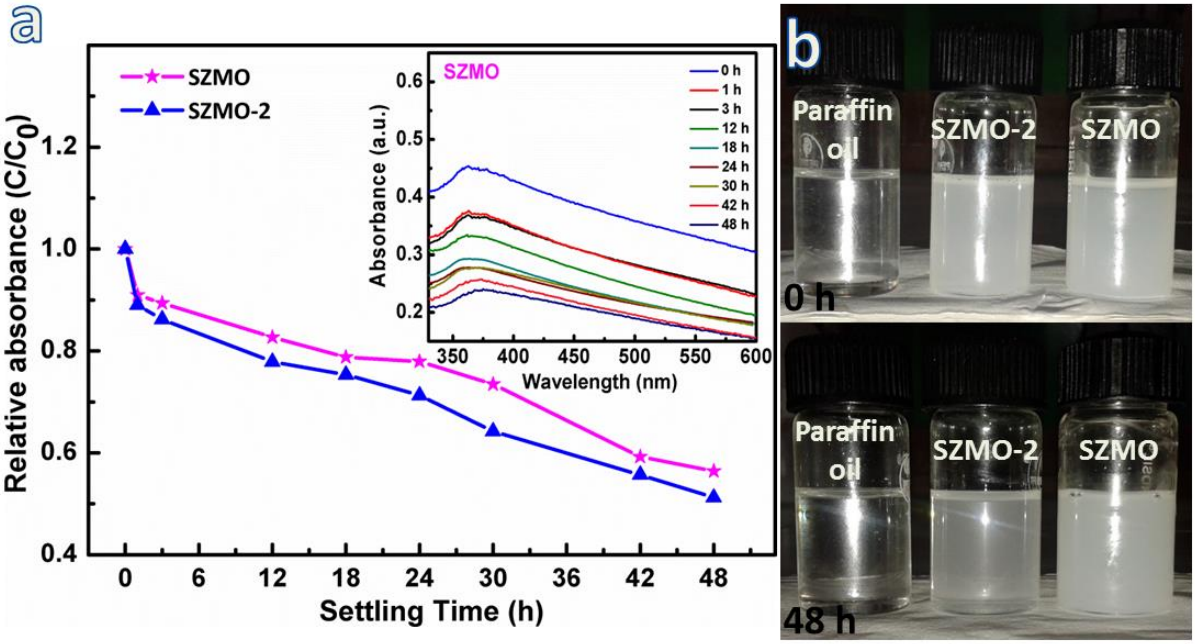

Figure 7.4.a. Relative absorbance of SZMO and SZMO-2 nanoparticles at different time interval and the UV-Visible spectra of SZMO nanoparticles at different settling times (in inset) and **(b).** Optical photographs of the different SZMOs NPs suspended in pure paraffin oil at different settling times

7.2. Results and discussion

7.2.1. Additive optimization

The lubrication properties of different SZMOs and SZnO NPs in paraffin oil have been evaluated on four ball tester machine. Figure 7.5 displays the optimization result for the SZMOs and SZnO NPs for different additive concentrations, load 392N, speed 1200 rpm and test duration 60 min. In absence of additives, the mean wear scar diameter (MWD) was found to be very large but in presence of SZMOs and SZnO NPs it was fairly reduced at each concentration. As the concentration of SZMO NPs in the base oil increases, the extent of reduction in the value of MWD also increases. On addition of 0.25% w/v SZMOs NPs to the base lube, huge reduction in the MWD values is observed. Thereafter, further increase in the concentration up to 1.00% w/v has little effect on the tribological behavior. Therefore, 0.25% w/v is an optimum concentration to provide significant friction and wear reduction. The reduction of MWD in presence of SZnO is comparatively much smaller than that in presence of SZMOs nanoparticles. Figure 7.5 reveals that SDS-stabilized Mg-doped-ZnO NPs performed better than those of pure zinc oxide.

7.2.2. Antiwear behavior

Figure 7.6 shows the changes in average coefficient of friction (COF) and mean wear scar diameter (MWD) in presence and absence of 0.25% w/v SZnO and SZMOs NPs in paraffin oil at constant load 392N. In general, on addition of nanoparticles to the paraffin oil, both the COF and MWD are significantly reduced. The mean wear scar diameter is larger in case of paraffin oil alone but in presence of different SZMOs and SZnO nanoparticles it appreciably reduces. The value of MWD is magnificently reduced in presence of SZMOs than SZnO NPs. Among the SZMOs NPs, the value of MWD and

average COF successively decreases for SZMO-2, SZMO-1 and SZMO. The values of MWD and COF were found to be the lowest for the surface supplemented with blend of SZMO NPs (27nm) whereas the largest MWD and COF values are observed in case of SZMO-2 (44nm) NPs. The lowering in both MWD and COF values in presence of SZMOs NPs is strongly size-dependent. This indicates that SZMOs NPs, when used as antiwear additives, play an important role in enhancing the tribological properties of paraffin oil.

Figure 7.7 exhibits the variation of coefficient of friction with sliding time at 392N applied load. In general, in presence of SZMOs NPs the value of COF gradually decreases with time and after some time it gets stabilized except for SZMO-2. The abnormal trend of SZMO-2 may be due to its larger particles size (44nm). Having larger particles size, SZMO-2 NPs tend to settle down in paraffin oil after some time due to gravity, this results in poor dispersion stability and therefore high COF values. Thus, the admixtures of SZMOs NPs in paraffin oil act as friction modifier except SZMO-2.

In order to study the wear rates, the tribological tests have been also conducted for paraffin oil at 392N applied load for different time durations 15, 30, 45, 60, 75 and 90 min. in presence and absence of nanoadditives. The behavior of MWD and mean wear volume (MWV) with time has been mentioned in Figure 7.8 and Figure 7.9. The plots of running-in and steady-state wear rates have been given in Figure 7.10 and Figure 7.11. The values of running-in and steady-state wear rates have been mentioned in Table 7.1 which clearly depicts that these values of wear rates are tremendously reduced in presence of SZMOs. The running-in wear rate is found to be larger than the steady-state wear rate. The lower value of steady-state wear rate is desirable as it is a measure of machine life. It has been observed that the reduction in the wear rate is also size-dependent and the value of steady-state wear rate is successively reduced to 69, 66 and 55 % respectively for SZMO, SZMO-1 and SZMO-2 NPs.

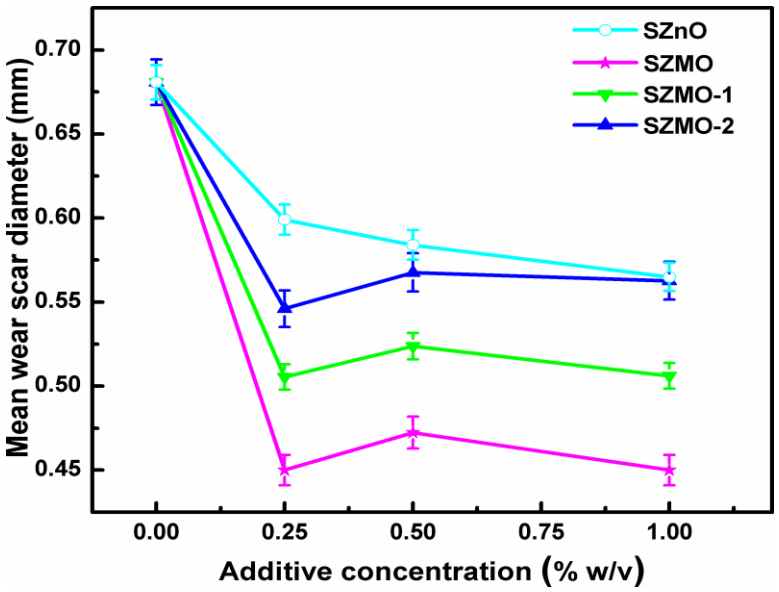

Figure 7.5. Variation of mean wear scar diameter in absence and presence of different additive concentrations in paraffin oil at 392N applied load and 60 min. duration

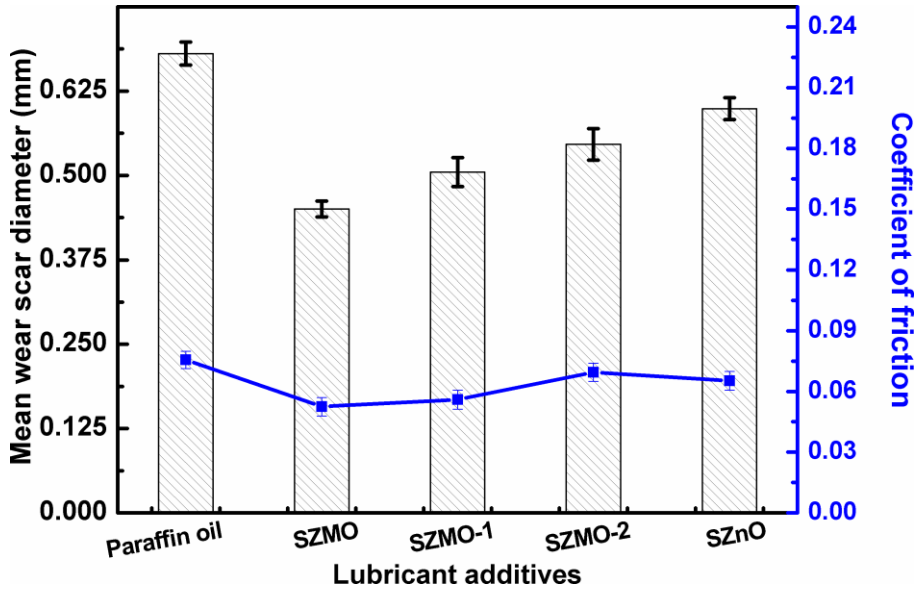

Figure 7.6. Comparison of MWD and COF of steel balls lubricated with different nanoparticles in paraffin oil at 392 N; rotating speed: 1200 rpm, temperature: 75 °C, test duration: 60 min., concentration: 0.25% w/v of nanoparticles

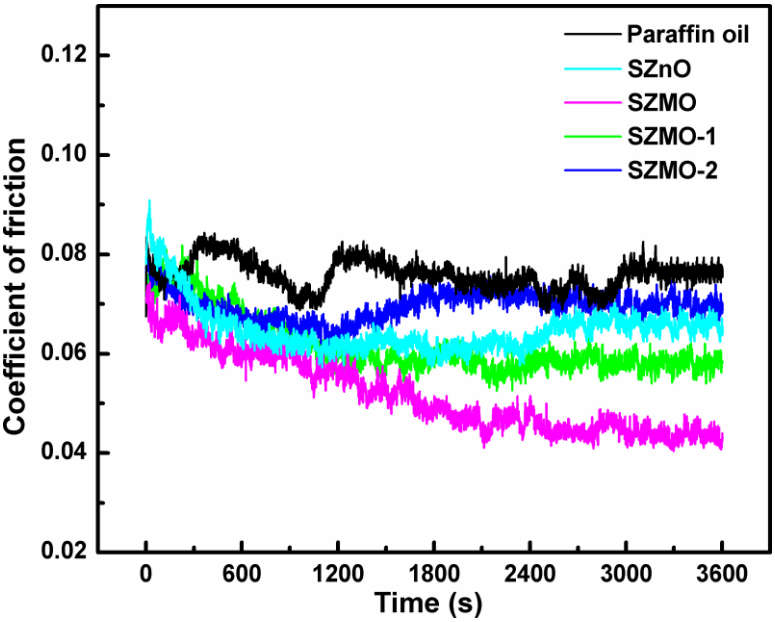

Figure 7.7. Variation of COF with sliding time in presence and absence of different nanoparticles in paraffin oil at 392N; rotating speed: 1200 rpm, temperature: 75 °C, test duration: 60 min., concentration: 0.25% w/v of nanoparticles

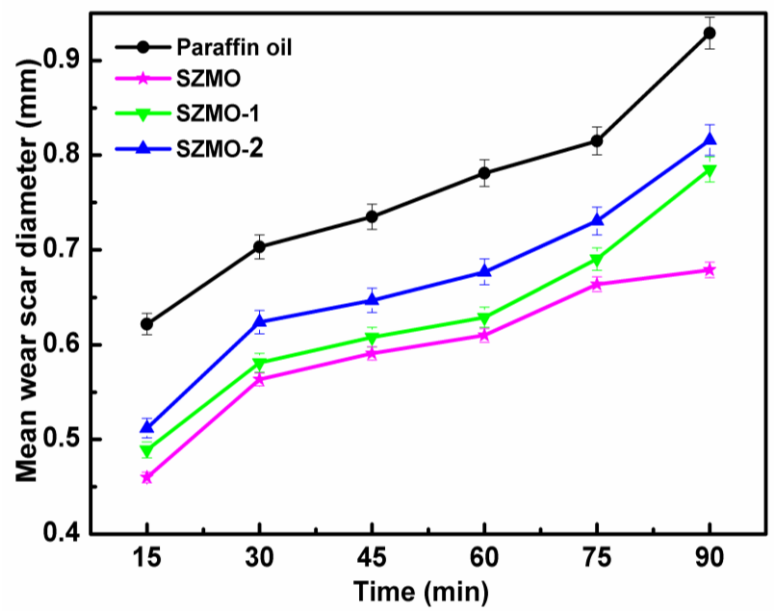

Figure 7.8. Variation of mean wear scar diameter with time in paraffin oil containing SZMOs nanoparticles at 392N applied load

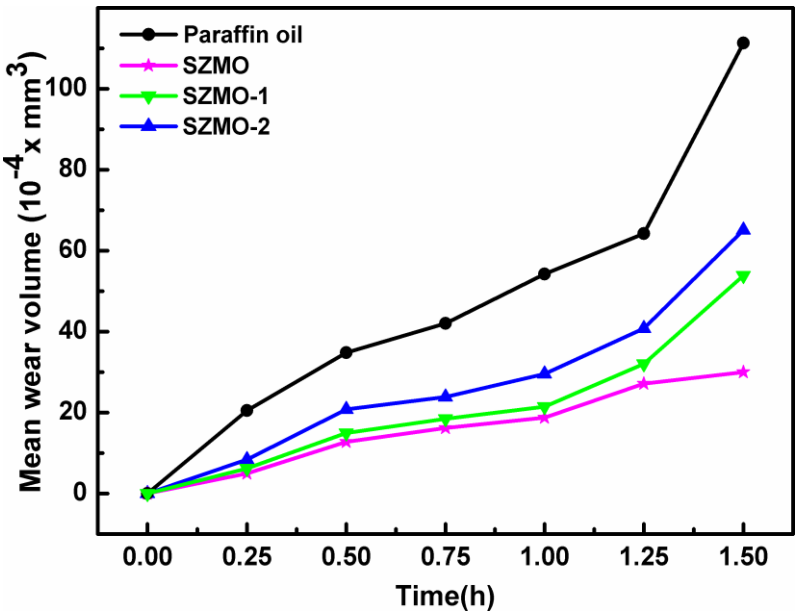

Figure 7.9. Variation of mean wear volume with time (h) in paraffin oil containing SZMOs nanoparticles at 392N applied load

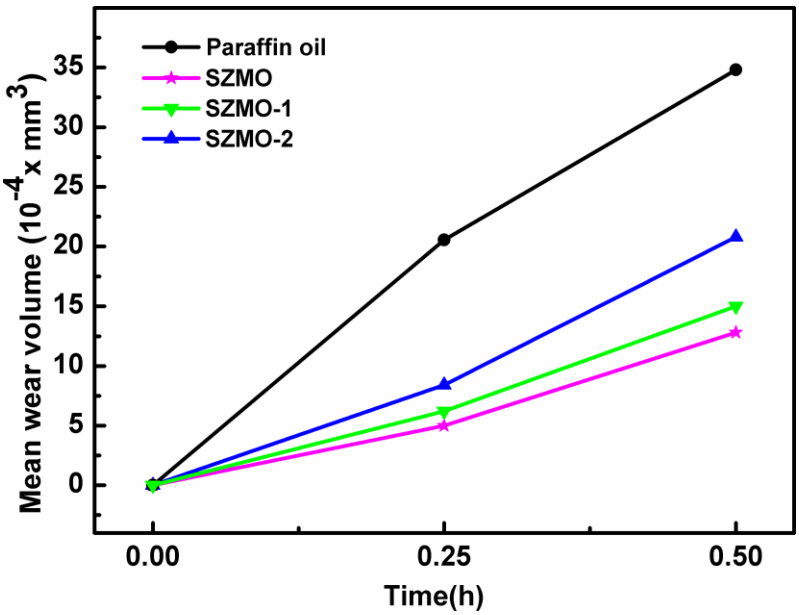

Figure 7.10. Determination of running-in wear rate by varying mean wear volume with time (h) for paraffin oil containing SZMOs nanoparticles at 392N applied load

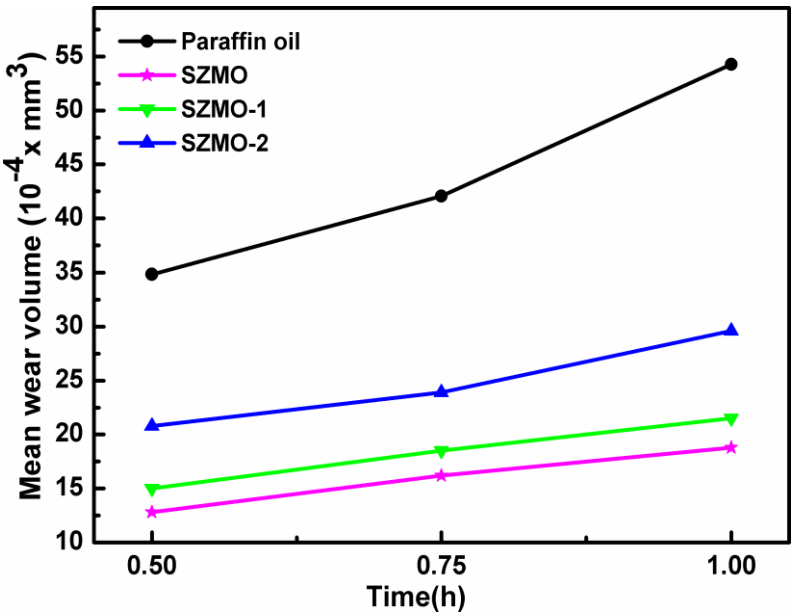

Figure 7.11. Determination of steady-state wear rate by varying mean wear volume with time (h) for paraffin oil containing SZMOs nanoparticles at 392N applied load

Table 7.1. Wear rates of paraffin oil in absence and presence of SZMOs nanoparticles as antiwear additives at 392N applied load for 90 min. test duration

S.N.	Additives	Wear Rate (10^{-4}x mm^3/h)	
		Running-in	Steady-state
1.	SZMO	25.60	12.00
2.	SZMO-1	30.00	13.00
3.	SZMO-2	41.60	17.60
4.	Paraffin oil	69.99	38.88

The performance of these additives as a function of load has been evaluated at different loads 294, 392, 490, 588 and 686N for 30 min. of test duration in paraffin oil,

Figure 7.12. The values of MWD at each load are higher in case of plain paraffin oil than those of its admixtures. It can be seen from the figure that the paraffin oil bears load only up to 490N whereas SZMO-1 and SZMO-2 NPs bear the load up to 588N. The smallest SZMO NPs successfully bear the load up to 686N. Being the smallest, these NPs act as a nanobearing and/or undergo tribosinterization in between the steel-steel interface and thus prevent the surfaces from adhesion [Battez *et al*.(2008) and Jaiswal *et al.*(2014)].

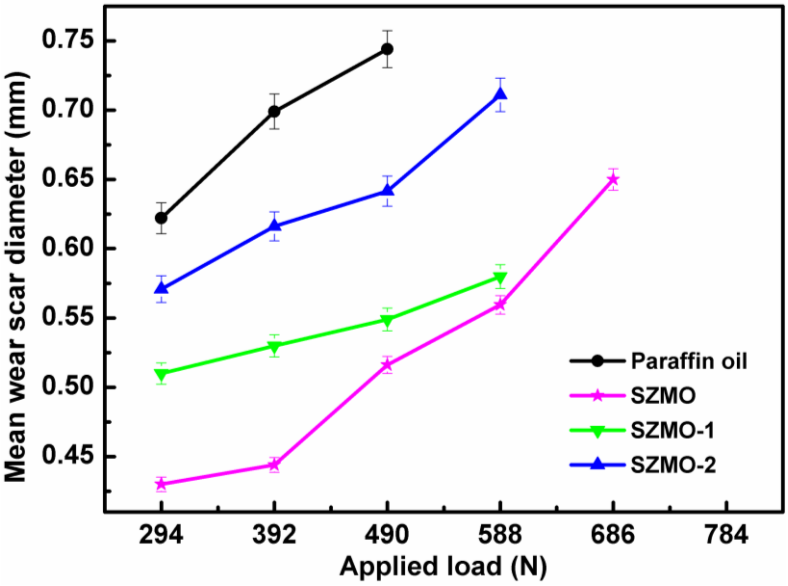

Figure 7.12. Variation of mean wear scar diameter with applied load for paraffin oil containing 0.25% w/v of SZMOs nanoparticles for 30 min. test duration

7.2.3. Coefficient of friction test

To investigate the COF behavior of these SZMOs NPs at steady-state zone, the friction test has been performed according to ASTM D5183. Figure 7.13 displays a load ramp test with the increment of 98N load at every 10 min. of test run (600 rpm; 75 °C) stepped from 98N up to 2254N for paraffin oil with and without additives. From the figure, it is apparent that the COF of paraffin oil increases drastically when the applied load

increases from 980 to 1078N whereas a very small increase in COF is observed in case of the tested nanoparticles for the same increment of load. It is evident that all these NPs are better friction modifiers, compared to the base oil. The SZMO NPs successfully carry the load up to 2254N with lower value of COF whereas SZMO-1 and SZMO-2 NPs bear the load only up to 2058, 1960N, respectively. These results indicate that the doped NPs are excellent friction modifiers and their behavior follows the same trend as observed in case of antiwear test.

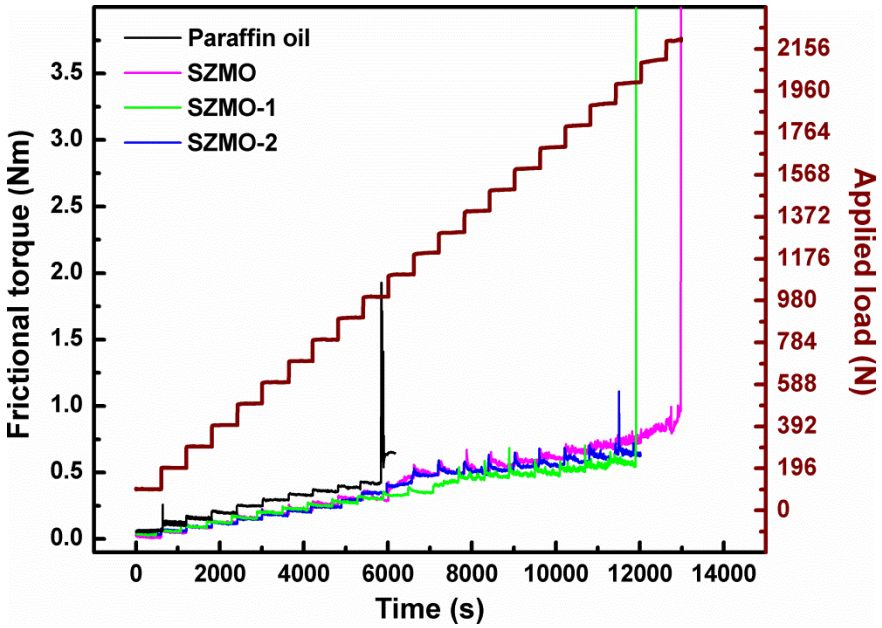

Figure 7.13. Variation of frictional torque as a function of step loading (with the increment of 98N load at every 10 min. of test run) and time for different SZMOs nanoparticles; sliding speed:600 rpm; temperature: 75 °C, additive concentration: 0.25% w/v

7.2.4. Proposed Mechanism

Since the friction and wear reducing properties of SZMOs NPs in paraffin oil are increased with the decrease in nanoparticles size, this indicates that the observed tribological behavior is size-dependent. Further, the superior tribological behavior of

SZMOs over SZnO NPs shows the effect of Mg-doping to ZnO. Thus, both of these characteristics (size and doping) are responsible for the enhanced tribological properties of ZnO. The Xie *et al*.(2010) have reported that the thermal conductivity of MgO NPs is 3.5 folds higher than that of ZnO NPs. Thus, it is expected that doping of Mg into ZnO might have increased thermal conductivity. As a result, these Mg-doped nanoparticles reduce the asperity temperature acting as coolant and finally resist adhesion. The antiwear mechanism of the investigated additives may follow four different processes: (i) the nanoparticles may melt, get welded on the interacting surfaces to form a tribofilm which may prevent direct asperity-asperity contact, or (ii) these may act as a third body on rubbing surfaces i.e. like nano-bearings and or (iii) these may get tribosintered on the surfaces under operating conditions and or (iv) these nanoparticles function as coolant which resist the increase in asperity-asperity temperature preventing welding [Battez *et al*.(2008)]. These SZMOs nanoparticles may follow all the aforesaid pathways except the first one because the melting temperatures of metallic nanoparticles are very high. Under lower load, these nanoparticles act as nanobearing and coolant. At higher loads, it may follow coolant, nanobearing and/or tribosinterization mechanism. However, with increase in load the amount of Zn and Mg on the worn surfaces also increases showing the tribosinterization mechanism is predominant at higher load which is evident from the EDX-analysis. Therefore, SZMOs NPs follow either nanobearings and/or tribosinterization mechanism and act as coolant at the steel-steel interface under operating conditions, minimizing metal-metal contact and thus friction and wear are reduced.

7.2.5. Surface Characterization

7.2.5.1. Surface morphology

The surface morphology of wear scar on steel ball surface lubricated with paraffin oil, SZMO (27 nm) and SZMO-2 (44 nm) at 392 N for 60 min. time duration was studied by scanning electron microscopy (ZEISS SUPRA 40) and Atomic Force Microscopy (Nanosurf easyscan2). The SEM images for the surface lubricated with paraffin oil show much wider wear scar due to severe scuffing apparent in Figures 14a,b. However, the width of the wear scar is smaller in size for the steel lubricated with blend of SZMOs nanoparticles, Figures 14c-f. These NPs filled the surface irregularities resulting into smoothening of surfaces. As expected from tribological studies, the MWD in case of SZMO is found to be quite smaller than that of SZMO-2 indicating its excellent AW properties. The SEM images of worn surface lubricated with and without additives at high load (490N) also support the results obtained in AW test, Figure 7.15.

Surface smoothness of the wear track lubricated with admixture of nanoadditives after the tribological tests was examined by contact mode AFM at 392N load for 60 min. test duration. The *2D* and *3D*-AFM images of the wear scar in presence of base oil and SZMOs NPs along with several roughness parameters are shown in Figure 7.16. From figure it is evident that area as well as line roughness are found to be extremely large (Sq= 556nm; Rq= 537nm) in case of paraffin oil whereas in presence of SZMO, SZMO-1 and SZMO-2 NPs (Sq= 47-95nm; Rq= 41-120nm) these have magnificently reduced. A large difference in the average peak-valley height is obtained for the tribopairs lubricated with paraffin oil alone (2.63μm) whereas very small surface irregularities are found in case of SZMOs (300-680 nm). These additives are capable in reducing area surface roughness up

to 91%. Thus, the AFM-images also proved the potential application of these Mg-doped-ZnO NPs towards minimizing friction and wear. The AFM-analysis of the steel ball lubricated with SZMOs NPs under the high load was also investigated and corresponding 2*D* and 3*D*-images are shown in Figure 7.17. As the load increases, the value of area-roughness, line roughness and also peak-valley height increases. The AFM-studies at high load also support the results obtained from SEM investigation under the similar test conditions.

7.2.5.2. Tribochemistry

In order to investigate the tribochemistry of paraffin oil and its blends with SDS-stabilized Mg-doped-ZnO nanoparticles, the EDX analysis has been performed. The EDX spectra of worn steel surface lubricated with 0.25% w/v of SZMO nanoparticles under 392N load have been shown and compared with the base lube. Figure 7.18a shows the prominent additional peaks for Zn and Mg elements on the worn surface lubricated with SZMO whereas these elements are completely absent in case of EDX spectra of surface lubricated with base oil shown in Figure 7.18b. The elemental analysis shows that distribution of Zn, Mg and O is throughout the surface of wear scar, Figure 7.19. The occurrence of constituents of additives on the sliding surface confirmed that the SZMO nanoparticles illustrate the referred tribosinterization mechanism. The atomic % of these elements for the surface supplemented with SZMO (27nm) and SZMO-2 (44nm) further increases as the load increases to 490N (Figure 7.20), this indicates that the tribosinterization phenomenon is predominantly favorable at high load. Under extreme conditions these nanoparticles may fill the valleys of interacting surfaces and rest of the nanoparticles act as a nanobearing thus preventing steel-steel interfaces from being welded.

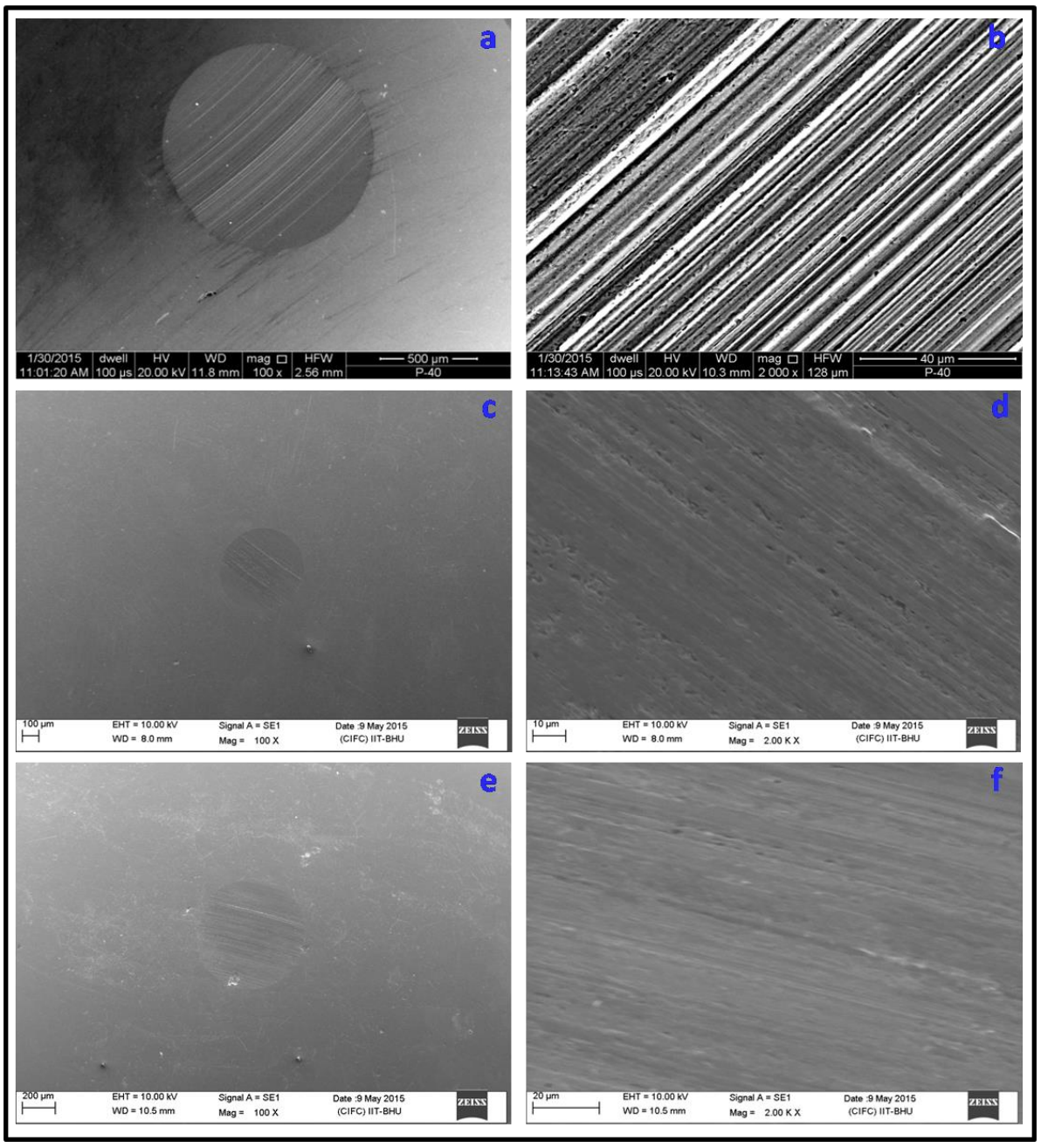

Figure 7.14. SEM micrographs of the worn steel surface lubricated with different nanoparticles in paraffin oil for 60 min. test duration at 392N applied load: **(a,b)**. Paraffin oil, **(c,d)**. SZMO and **(e,f)**. SZMO-2 nanoparticles

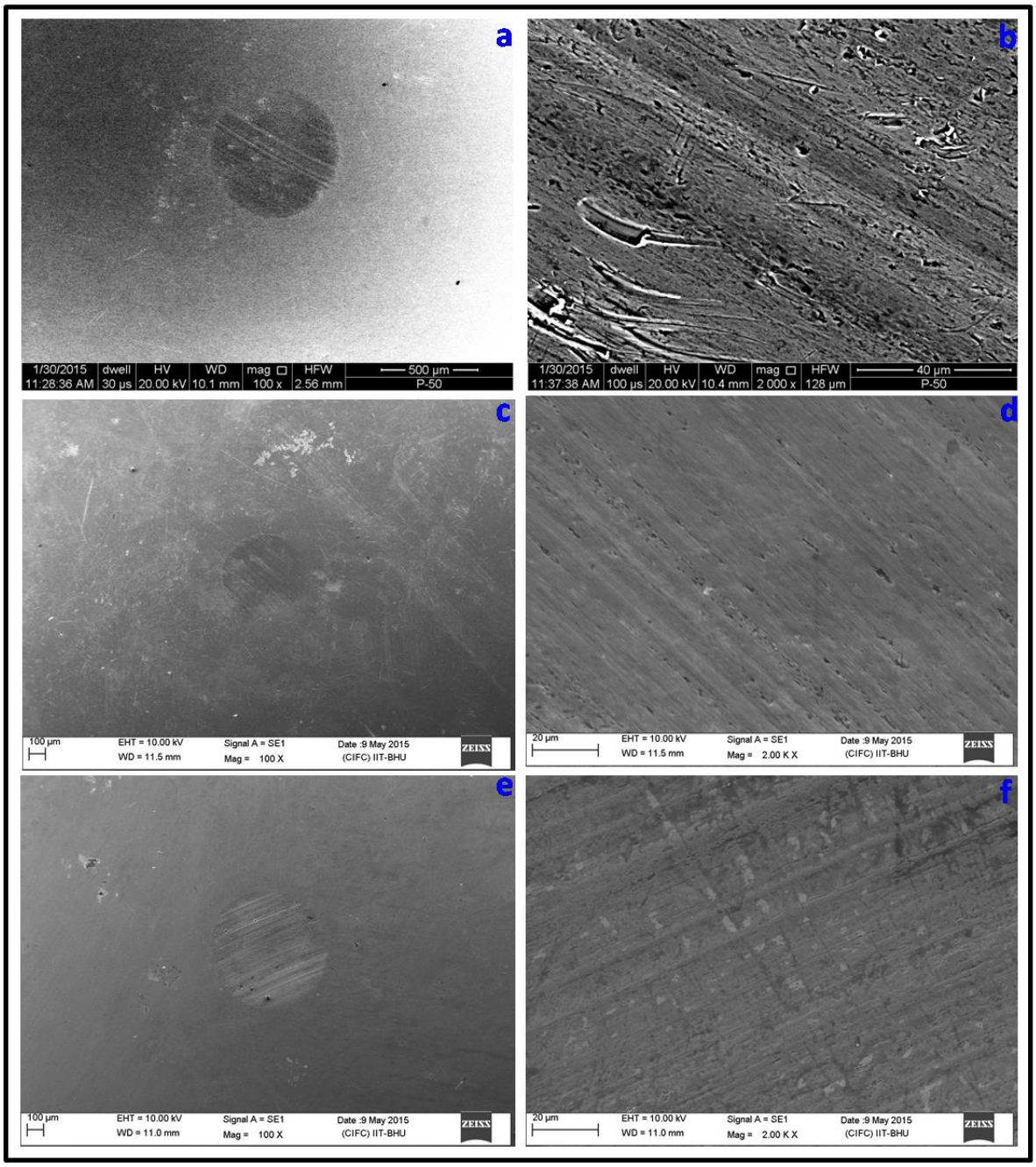

Figure 7.15. SEM micrographs of the worn steel surface lubricated with different nanoparticles in paraffin oil for 30 min. test duration at 490N applied load: **(a,b)**. Paraffin oil, **(c,d)**.SZMO and **(e,f)**.SZMO-2 nanoparticles

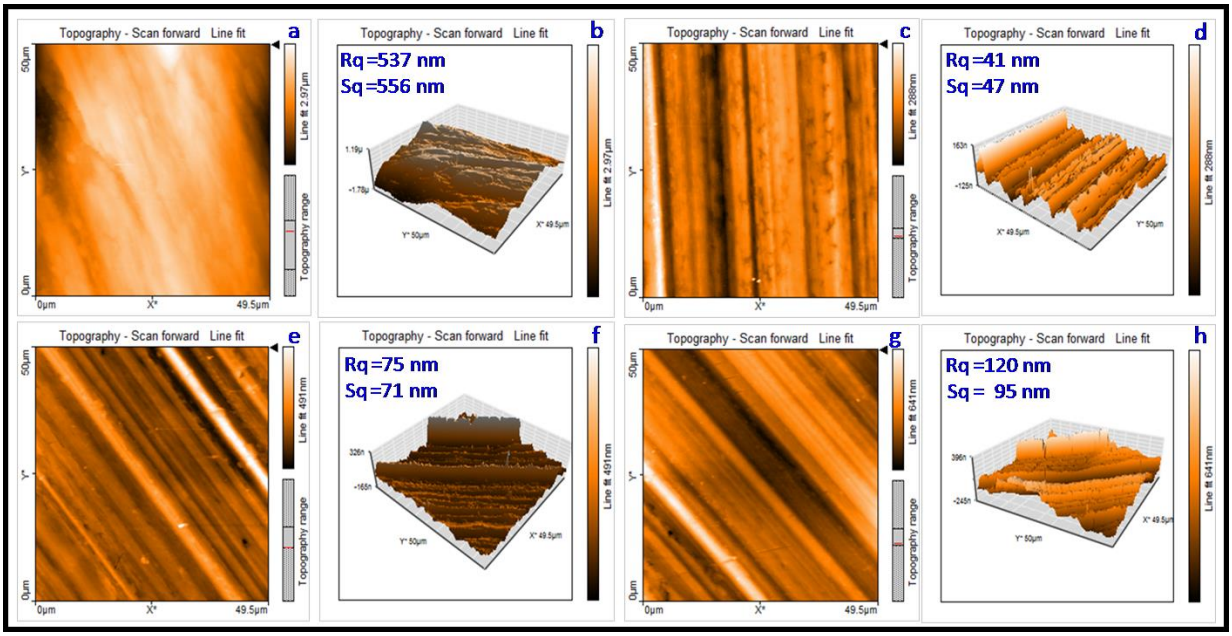

Figure 7.16. 2*D* and 3*D*-AFM images of the worn steel surface lubricated with different additives in paraffin oil for 60 min. test duration at 392N applied load: (a,b). Paraffin oil, (c,d). SZMO, (e,f). SZMO-1 and (g,h). SZMO-2 nanoparticles

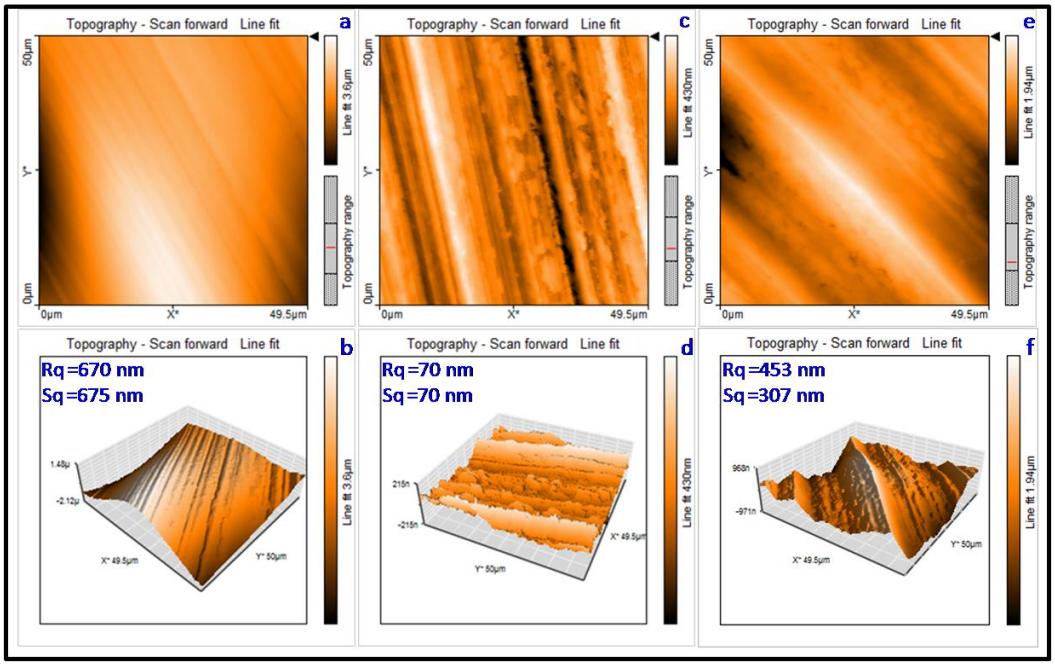

Figure 7.17. 2*D* and3*D*-AFM images of the worn steel surface lubricated with different additives in paraffin oil for 30 min. test duration at 490N applied load: **(a,b)**. Paraffin oil, **(c,d)**. SZMO and **(e,f)**. SZMO-2 nanoparticles

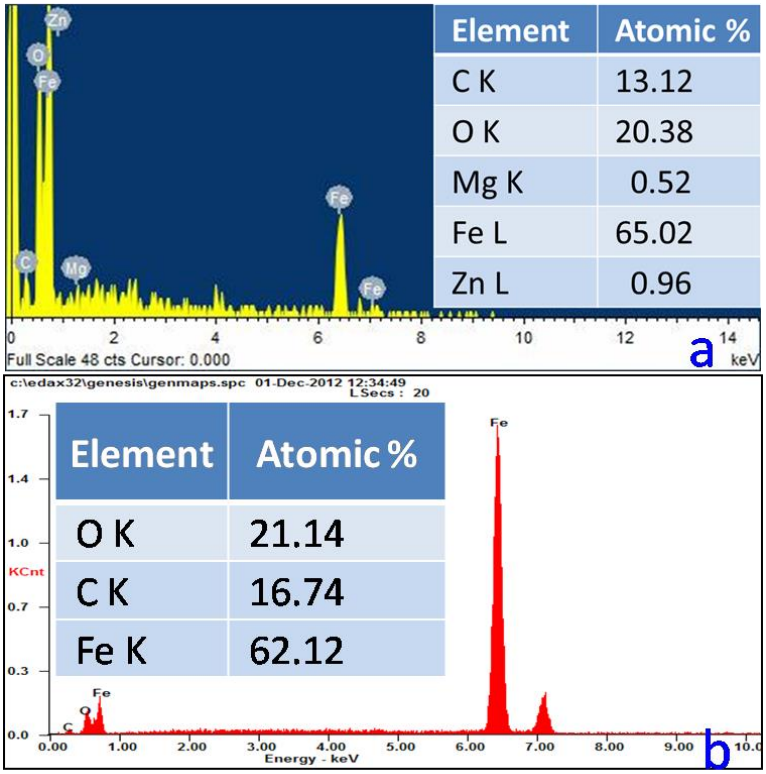

Figure 7.18. EDX analysis data of the worn steel surface lubricated with paraffin oil in presence and absence of different additives for 60 min. test duration at 392N applied load: **(a)**.SZMO nanoparticles and **(b)**. Paraffin oil

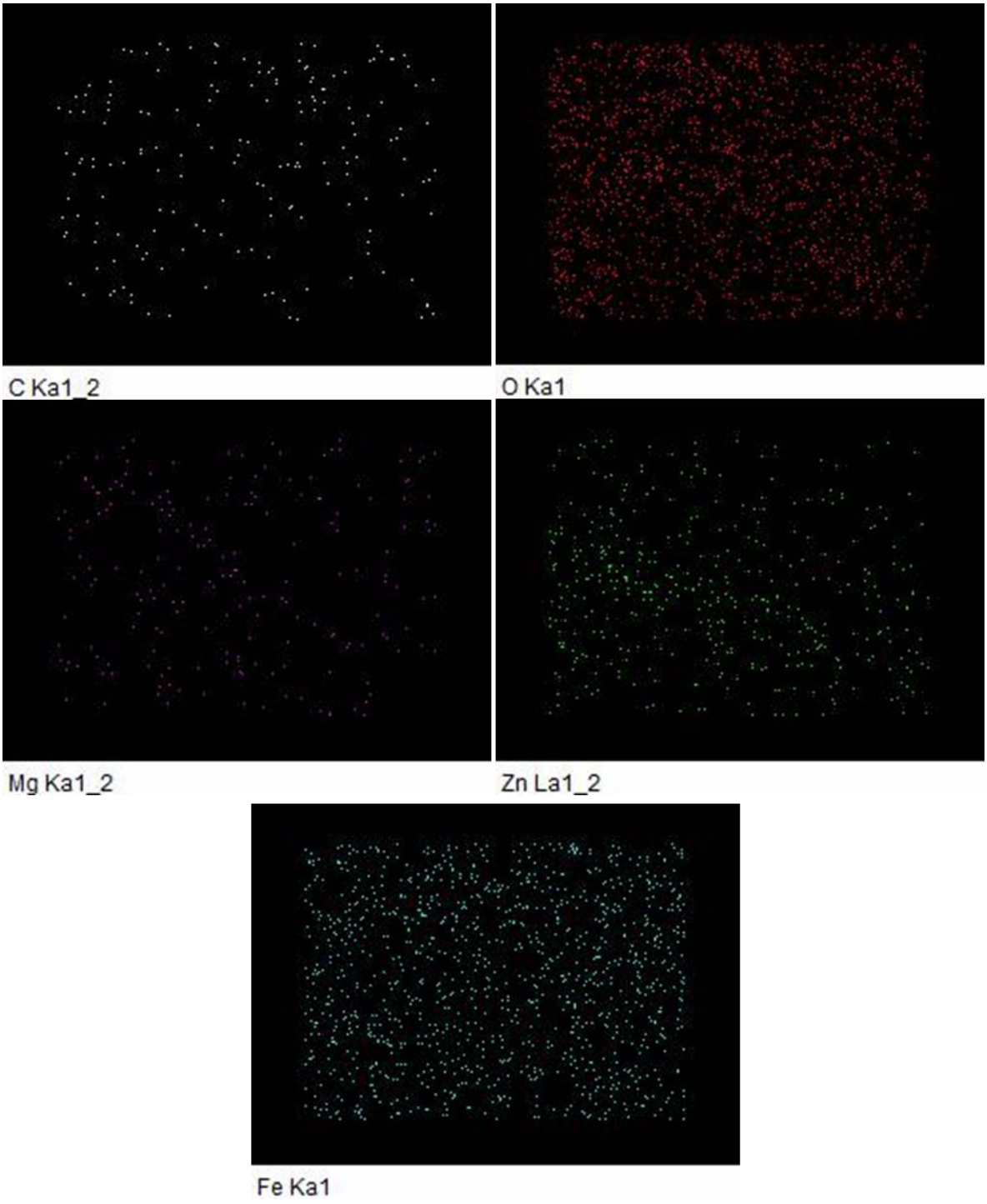

Figure 7.19. Elemental mapping of the various elements on worn steel surface lubricated with SZMO nanoparticles for 60 min. test duration at 392N applied load; (a). C, (b). O, (c). Mg, (d). Zn and (e). Fe

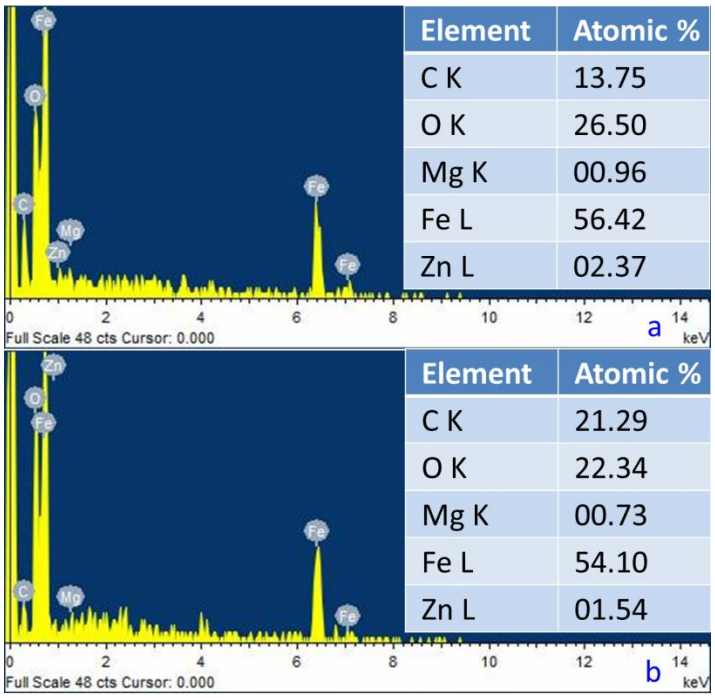

Figure 7.20. EDX analysis data of the worn steel surface lubricated with paraffin oil in presence of different nanoparticles for 30 min. test duration at 490N applied load: **(a)**. SZMO and **(b)**. SZMO-2

7.3. Conclusions

In summary, the Magnesium-doped zinc oxide ($Zn_{0.88}Mg_{0.12}O$; ZMO) nanoparticles were successfully prepared by auto-combustion method and the variation in particle size of ZMOs NPs was made by further increasing the temperature. Formation of doped nanoparticles was confirmed by XRD which correlates very well with the SAED pattern of TEM images. The crystallite size of SZMO nanoparticles was found to be 27, 39 and 44 nm for SZMO, SZMO-1 and SZMO-2, respectively. The suspension stability of blends of 0.10% SDS with ZMOs nanoparticles in paraffin oil was confirmed from UV-Visible spectra and it remains almost unaffected up to 48 hours. The blends of SZMOs nanoparticles show better antiwear properties than SZnO nanoparticles. The SZMO

nanoparticles as additives in paraffin oil exhibited excellent friction-reduction, antiwear and load carrying property in the order of decreasing particle size. The running-in and steady-state wear rates of SZMOs nanoparticles have been found to be much lower than paraffin base oil. The SEM and AFM studies also support the results obtained from tribological studies. EDX analysis shows the presence of Zn and Mg elements on the sliding surface emphasizing the role of these additives in enhancing lubrication. Thus, being free from sulfur, phosphorous and halogens, these novel nanoparticles exhibit excellent tribological properties and have potential to be developed as low SAPS antiwear additives for boundary lubrication conditions.